

Physical mechanism of secondary-electron emission in Si wafers

Yanan Zhao(赵亚楠), Xiangzhao Meng(孟祥兆), Shuting Peng(彭淑婷), Guanghui Miao(苗光辉), Yuqiang Gao(高玉强), Bin Peng(彭斌), Wanzhao Cui(崔万照), and Zhongqiang Hu(胡忠强)

Citation: Chin. Phys. B, 2024, 33 (**4**): 047901. DOI: 10.1088/1674-1056/ad1175
Journal homepage: http://cpb.iphy.ac.cn; http://iopscience.iop.org/cpb

What follows is a list of articles you may be interested in

Thin film micro-scaled cold cathode structures of undoped and Si-doped AlN grown on SiC substrate with low turn-on voltage

Shi Ming (侍铭), Chen Ping (陈平), Zhao De-Gang (赵德刚), Jiang De-Sheng (江德生), Zheng Jun (郑军), Cheng Bu-Wen (成步文), Zhu Jian-Jun (朱建军), Liu Zong-Shun (刘宗顺), Liu Wei (刘炜), Li Xiang (李翔), Zhao Dan-Mei (赵丹梅), Wang Qi-Ming (王启明), Liu Jian-Ping (刘建平), Zhang Shu-Ming (张书明), Yang Hui (杨辉)
Chin. Phys. B, 2015, 24 (**5**): 057901. DOI: 10.1088/1674-1056/24/5/057901

Theoretical research on electron beam modulation in a field-emission cold cathode electron gun

Li Xing-Xing (李兴兴), Yuan Xue-Song (袁学松), Zhang Yu (张宇), Yan Yang (鄢扬)
Chin. Phys. B, 2014, 23 (**3**): 037901. DOI: 10.1088/1674-1056/23/3/037901

A comparison of the field emission characteristics of vertically aligned graphene sheets grown on different SiC substrates

Chen Lian-Lian (陈莲莲), Guo Li-Wei (郭丽伟), Liu Yu (刘宇), Li Zhi-Lin (李治林), Huang Jiao (黄郊), Lu Wei (芦伟)
Chin. Phys. B, 2013, 22 (**10**): 107901. DOI: 10.1088/1674-1056/22/10/107901

Research on field emission mechanism of nano-structured carbon film

Wang Yan-Yan (王艳燕), Li Ying-Ai (李英爱), Xu Ji-Song (许基松), Gu Guang-Rui (顾广瑞)
Chin. Phys. B, 2012, 21 (**8**): 087902. DOI: 10.1088/1674-1056/21/8/087902

Field emission properties of capped carbon nanotubes doped by alkali metals:a theoretical investigation

Jin Lei(靳磊), Fu Hong-Gang(付宏刚), Xie Ying(谢颖), and Yu Hai-Tao(于海涛)
Chin. Phys. B, 2012, 21 (**5**): 057901. DOI: 10.1088/1674-1056/21/5/057901

Physical mechanism of secondary-electron emission in Si wafers

Yanan Zhao(赵亚楠)[1,†,‡], Xiangzhao Meng(孟祥兆)[1,†], Shuting Peng(彭淑婷)[1], Guanghui Miao(苗光辉)[2,3], Yuqiang Gao(高玉强)[4], Bin Peng(彭斌)[1], Wanzhao Cui(崔万照)[2], and Zhongqiang Hu(胡忠强)[1]

[1] *State Key Laboratory for Manufacturing Systems Engineering, Electronic Materials Research Laboratory, Key Laboratory of the Ministry of Education, Engineering Research Center of Spin Quantum Sensor Chips, Universities of Shaanxi Province, School of Electronic Science and Engineering, Xi'an Jiaotong University, Xi'an* 710049, *China*

[2] *College of Aeronautics, Nanjing University of Aeronautics and Astronautics, Nanjing* 210016, *China*

[3] *National Key Laboratory of Science and Technology on Space Microwave, China Academy of Space Technology (Xi'an), Xi'an* 710100, *China*

[4] *Department of Physics, School of Physics and Electronic Information, Anhui Normal University, Wuhu* 241000, *China*

(Received 18 September 2023; revised manuscript received 7 November 2023; accepted manuscript online 1 December 2023)

CMOS-compatible RF/microwave devices, such as filters and amplifiers, have been widely used in wireless communication systems. However, secondary-electron emission phenomena often occur in RF/microwave devices based on silicon (Si) wafers, especially in the high-frequency range. In this paper, we have studied the major factors that influence the secondary-electron yield (SEY) in commercial Si wafers with different doping concentrations. We show that the SEY is suppressed as the doping concentration increases, corresponding to a relatively short effective escape depth λ. Meanwhile, the reduced narrow band gap is beneficial in suppressing the SEY, in which the absence of a shallow energy band below the conduction band will easily capture electrons, as revealed by first-principles calculations. Thus, the new physical mechanism combined with the effective escape depth and band gap can provide useful guidance for the design of integrated RF/microwave devices based on Si wafers.

Keywords: secondary-electron yield, doping concentration, escape depth, Si wafer

PACS: 79.70.+q, 85.40.Ry, 61.85.+p, 81.05.Ea **DOI:** 10.1088/1674-1056/ad1175

1. Introduction

Secondary-electron emission, known as a secondary-electron avalanche, refers to the phenomenon of electrons escaping from the surface of materials when particles are bombarded with a certain initial energy.[1–5] A high secondary-electron yield (SEY) is required for scanning electron microscopy, particle accelerators and micro-channel plate detectors.[6–10] However, it results in performance degradation or even permanent damage in satellite microwave components and accelerators.[11–14] Thus, research on suppression of the SEY has received considerable attention.

Most researchers have concentrated on surface treatment techniques,[15–19] such as the formation of grooved,[20–22] fibrous[23,24] and micro-porous[25] structures. However, the SEY increases after surface treatment of the sinusoidal rippled surface[26] and the larger triangular grooves.[27,28] Another approach involves coating with low-SEY materials in RF/microwave equipment. Luo *et al.*[29] discovered an ultra-low SEY by coating a one-atom-thickness graphene film, which has good electronic and thermal conductivity.[30] However, the complexity of the high-quality-transfer graphene process and the weak adhesion to the substrate greatly limit the practical applications of graphene films. B/N doped-silicon (Si) wafers are suitable candidates for RF/microwave devices due to their tunable conductivity, low cost, chemical stability and easy-to-scale fabrication process. Meanwhile, strained silicon technology involves the use of various means to physically stretch or compress silicon crystals, which increases carrier (electron, hole) mobility and enhances transistor performance in turn.[26,31,32] In addition, Dionne *et al.* have proposed a semi-empirical model to describe the dependence of the initial electron transmission depth on the initial electron energy[33] using first-principles calculations, which is especially suitable for analyzing the conductive mechanism of Si wafers with different doping concentrations.

In this paper, we have demonstrated the SEY suppression phenomenon in silicon wafers with different doping concentrations, and have proposed a physical mechanism based on conductivity and band gap using first-principles calculations. An unexpected finding is that the effective escape depth λ of the inner secondary electrons is negatively correlated with the conductivity of the silicon wafer. The optimal N-doped silicon wafer has a minimum SEY coefficient of 1.98 and a minimum band gap (E_g) of 0.511 eV from first-principles calculations.

2. Experimental detail

Silicon wafers with different concentration ranges of dopant were purchased from Virginia Semiconductor. The square resistance of the samples was tested using a four-probe resistance system. After the square resistance was obtained,

†These authors contributed equally to this work.
‡Corresponding author. E-mail: zhaoyanan1984@xjtu.edu.cn

© 2024 Chinese Physical Society and IOP Publishing Ltd

the resistivity of the Si wafers was calculated using the formula $\rho = R \times t$ (where t stands for the thickness of the Si wafers). Figure 1(a) shows the SEY test system and its equivalent circuit diagram. We applied a bias voltage of +500 V to the bottom of the samples, and then shot an electron beam of a certain energy with an electron gun. The total electron beam I_p was measured. A bias voltage of −20 V was applied on the bottom of the samples, and the current I_s was measured, except for the secondary-electron beam. Then, the SEY of the samples was obtained using the formula in Refs. [34–37]. In the test process, the SEY curves were measured multiple times to ensure consistency and integrity, to avoid the effects of charge effects on the SEY

$$\delta = (I_p - I_s)/I_p. \tag{1}$$

Here, the structure optimization and energy-band structure calculations of doped Si wafers were completed using the CASTEP module in Material Studio software,[38] which is based on the generalized gradient approximation (GGA) with the Perdew–Burke–Ernzerh (PBE) function. The calculated concentration was evaluated at low, medium, and high ACC concentrations (0.781%, 1.562%, and 3.125%) in samples using mean data provided by the manufacturer in ranges of (0%–1%, 1%–2%, and 2%–4%).

For all the calculations, the ultra-soft pseudopotentials were used. The cut-off energy of 220 eV was assumed in the plane-wave basis set. For the k-point integration, we used a $2 \times 2 \times 4$ mesh for the cubic unit cell of Si, and structure relaxation was performed until the convergence criteria of 2.0×10^{-5} eV/atom. The maximum stress was 0.1 GPa, and the maximum ionic displacement was 0.002 Å. Here, the spin polarization was not taken into consideration in the calculations.

3. Results

Figures 1(b) and 1(c) show the SEY curves of doped Si wafers of different types and concentrations as a function of the primary electron energy E_0 from 0 to 1600 eV at the normal incident. As the B-doped concentration increases, the δ_m gradually becomes low in Fig. 1(b), yet they are almost the same in medium and highly doped Si wafers. The suppression process of the SEY in B-doped Si wafers is instability, in which the effect induced by the doped holes may exceed that of the same number of doped electrons. As the N-doped concentration increases, Fig. 1(c) shows the continual decline of δ_m in N-doped Si wafers. The effects induced by doping concentrations of Si wafers principally include two modes: electrical conductivity and electron–impurity scattering. The latter is beneficial in suppressing the SEY. There is a net electron flow from the emission samples into the vacuum when δ is greater than 1, in which a certain conductivity inside the samples will supplement the lost electrons.[34]

The variation trend is related to the escape depth λ of internal secondary electrons, and λ obeys the law of power exponent absorption among the electron multiplication process based on the electronic cascade model.[33,38,39] A semi-empirical theory (Dionne model) of SEY to describe the SEY curve is as follows:[35,36,40]

$$\delta = \frac{B}{E_a}(An\lambda)^{1/n}\left(\frac{d_m}{\lambda}\right)^{\frac{1-n}{n}}(1 - e^{-d_m/\lambda}), \tag{2}$$

$$\delta_m = 0.9\frac{B}{E_a}(\lambda A)^{0.74}, \tag{3}$$

$$E_m = 2.3(\lambda A)^{0.74}, \tag{4}$$

$$d_m = E_0^n/(An). \tag{5}$$

Here, B is the escape probability, defined as the constant without any surface treatment; E_a is the required activation energy; A is a constant characteristic of the material, directly due to the right doping ratio below 5%; n (1.35 for semiconductor[41]) is the power exponential decay factor depending on the material; d_m represents the maximum[42] relative to the initial electron energy E_0. Here, λ^{-1}, described as the secondary-electron absorption coefficient or inverse mean free path, is ascribed to conductivity in the Dionne model. The fitting curves of N-doped samples, as shown in Fig. 1(c), are in accord with the experimental results. Therefore, the escape depth λ is the only factor to affect the value of δ in Eq. (2). Thus, we can calculate the value of λ from the experimental results of the SEY curves, as shown in Table 1, where E_m is the energy as the maximum yield coefficient δ_m occurs. Here, the value of λ is in the same order of magnitude as the penetration depth.[39,43]

In our work, Fig. 2(a) shows the conductivity values of N-doped silicon wafers with different concentrations from 15 S/m to 1666 S/m. Figure 2(b) reveals the trend of δ_m and the effective escape depth λ with the conductivity of N-doped silicon wafers. As the conductivity increases, the value of δ_m decreases from 2.53 to 1.98, and the corresponding value of λ decreases from 9.1 to 4.0. Statistical analysis reveals that there is a negative correlation between δ_m and the conductivity of the material (especially semiconductor materials). Therefore, to obtain a lower SEY, one can focus on materials with higher conductivity. Scattering between electron phonons and impurities may reduce the escape depth of internal secondary electrons, which is the main cause of secondary-electron energy loss. Previous studies have discussed the effects of doping concentrations, and their results show a similar trend to ours.[44]

However, the B-doped Si wafers show a little mismatching compared with the N-doped samples. This is probably caused by the transformation of the scattering mechanism, in which a small number of carriers are effective enough to modulate the SEY of B-doped Si wafers. This infers that electron–hole scattering is the main channel of energy loss.

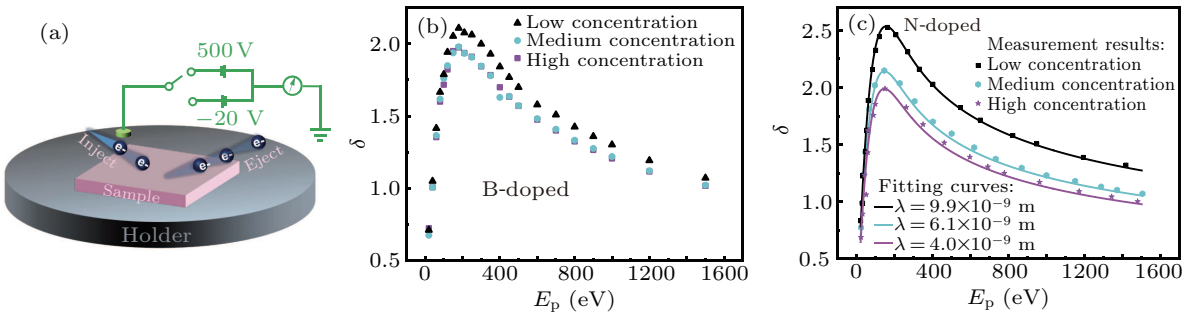


Fig. 1. (a) A schematic diagram of the secondary-electron emission test system. (b) SEY curves of Si wafers with different B-doping concentrations, in which the black triangles, cyan circles, and purple squares represent low, medium, and high concentrations, respectively. (c) SEY curves of Si wafers with different N-doping concentrations, in which the black circles, cyan rhombus, and purple pentagons represent low, medium, and high concentrations, respectively. The solid points show the measurement results, and the solid lines show the fitted curves from the Dionne model.

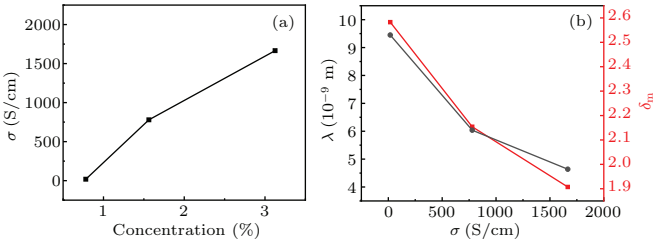


Fig. 2. (a) The conductivity σ as a function of different N-doped concentrations in Si wafers. (b) The average escape depth of inner secondary electrons versus the conductivity of doped Si wafers.

For a quantitative description of the SEY, the Monte Carlo method combined with scattering cross-section calculations would be the primary option.[45] However, because of the low doping concentration of our samples in the range between 0.781% and 3.125%, the doping systems (B(N)-doped Si wafers) constructed for the Monte Carlo simulations would be too large to properly account for the electron scattering by the impurities, which is computationally costly. Therefore, we theoretically studied the physical mechanism of N substitution in Si using first-principles calculations, and then experimentally investigated its effect on the structural and electrical properties. Here, the density of states, charge distribution, and the band structure were investigated using the density functional theory (DFT) method. The band structures of N-doped Si with three concentrations are shown in Figs. 3(a)–3(d). The theoretical calculation of the actual size of the semiconductor band gap involves the excited state theory. Generally, the quasi-particle GW correction of the band gap is needed. Here, the corrected band gap of pure Si by the scissor operation is 1.12 eV. It is consistent with the actual observation value.[46] In our work, the highly doped sample is an indirect band-gap semiconductor. Here, the valence band maximum (VBM) lies at the G point, whereas the conduction band minimum (CBM) is located at the Q point, which is not at the high-symmetry points of the first Brillouin zone. Table 1 shows that the optical band gap decreases with the increasing N doping concentration, which is favorable for suppressing the SEY. The band-gap results are approximately 1071 meV, 872 meV, and 611 meV for the slight, moderate, and heavy-doped concentrations, respectively.

To clearly see the change in band gaps for Si super-cells with different N-related defects, the Fermi level is set to zero in these band structures. There is an unambiguous relationship between E_g and impurity size, and the discrepancy may be attributed to the different levels of electron impurity scattering from the phonon lattice vibrations. Therefore, this will induce restrictions on the escape depth of internal secondary electrons with kinetic energy less than the band-gap energy. In this simplified model,[47] reducing the bandgap width will not only increase the capture of electrons, but will also increase the probability of internal secondary-electron excitation. It increases the collision probability between the secondary electrons and the valence electrons in doped samples, in which the excitation of the core-shell and valence electrons in an inelastic scattering event consumes the kinetic energy of the energetic moving electron. Thus, inhibiting the SEY of doped samples is a complex impact process based on a combination of several factors. According to the test results of secondary-electron yields and the fitting results of the escape depth, electron traps are more likely to capture electrons due to the absence of shallow energy bands, and it should be the main factor to inhibit the SEY in doped samples.

Table 1. Secondary-electron parameters of Si samples.

	Sample	Concentration (%)	δ_m	E_m (eV)	λ (10^{-9} m)	σ (S/cm)	E_g (eV)
N-doped	low concentration	0.781	2.53	148	9.91	18	1.071
	medium concentration	1.562	2.14	141	6.16	779	0.872
	high concentration	3.125	1.98	138	4.00	1666	0.611
B-doped	medium concentration	1.562	1.965	177	4.31	1093	0.710

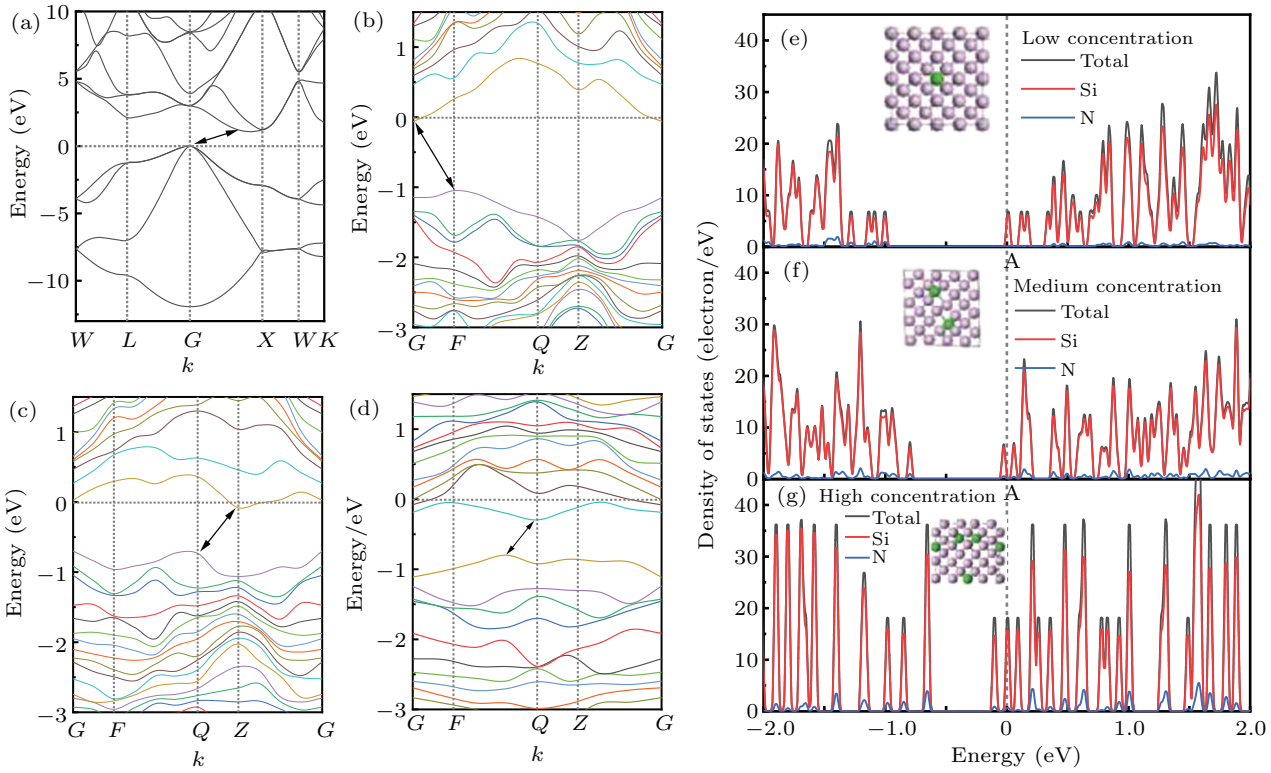


Fig. 3. Bands and structures of the super-cells with different N-doped levels: (a) pure Si, (b) low concentration, (c) medium concentration, (d) high concentration. Atomic geometry of super-cells with different N-doped levels after geometry optimization. Purple and green spheres indicate Si and N atoms, respectively. TDOS and PDOS of the super-cells with different N-doped levels: (e) low concentration, (f) medium concentration, (g) high concentration.

The computed partial density of states (PDOS) and total density of states (TDOS) are shown in Figs. 3(e)–3(g). The whole bands shift to the lower energy side with the increase in doping concentrations, and the impurity bands contributed by doped atoms are under the conduction band. Thus, this indicates a narrow band gap. Here, E_g values of 0.971 eV, 0.772 eV, and 0.511 eV are in good agreement with the computational results. The work function can be calculated as follows:[48]

$$\varphi = E_{VAC} - E_F, \tag{6}$$

where E_{VAC} and E_F are the vacuum energy and Fermi energy, respectively. Therefore, N doping will inevitably cause a decrease in the Fermi energy level, leading to an increase in the work function in the escape work. The surface barrier plays a significant role in the secondary-electron emission; thus, it responds to the suppression of the escape of secondary electrons as the N-doping concentration increases.

As shown in Figs. 3(e)–3(g), the impurity level will be formed in the bandgap of Si crystal when N is doped. With the increase in the doping concentration, the peak of the impurity energy level gradually increases. Meanwhile, with the increase in the Si doping concentration, the degeneracy is eliminated and the width of the impurity peak expands. When the impurity energy level is close to the bottom of the conduction band, the valence electrons are more easily excited and likely to produce intrinsic scattering. Meanwhile, the electrons easily develop into free electrons to move in the conduction band of the high N-doped concentration, as shown in Fig. 3(g). Moreover, the electronic cascade process only excites the electrons in the valence band to the vacuum level. As a result, electron traps are more likely to capture electrons due to the absence of shallow energy bands below the conduction band. This will lead to the suppression of the SEY because of the difficulty of excitation from the impurity level. The top of the valence band and the bottom of the conduction band play a key role in interpretation of the suppression of the SEY.

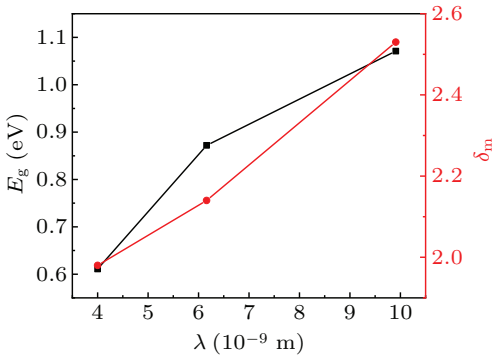


Fig. 4. The band energy gap E_g, the maximum value of SEY δ_m, and a function of the different mean free path λ of N-doped Si.

Figure 4 shows the dependency relationship among E_g, δ_m and the effective escape depth λ. The high N-doped Si has a relatively low E_g of 0.511 eV and the lowest λ of 4×10^{-9} m,

which is favorable for suppressing SEY. In general, the impurity energy level of N-doped Si is close to the conduction band, and it could be considered as an electron trap by the first-principles methods. It reduces the escape depth λ of the internal secondary electrons, in which case the kinetic energy is less than the bandgap energy due to the added electron–electron scattering.

4. Conclusion

We have shown that the secondary-electron yield of doped Si wafers depends critically on the doping types and concentrations. The secondary-electron yield is slightly suppressed by electron-impurity scattering, and the kinetic cascade emission process is promoted by the supplement of electrical conductivity. The physical mechanism of secondary-electron emission in Si wafers will provide guidance in the applications of high-power space RF/microwave devices.

Acknowledgements

Project supported by the Administration of Science, Technology and Industry of National Defense of China (Grant No. HTKJ2021KL504001), the National Natural Science Foundation of China (Grant Nos. 12004297 and 12174364), the China Postdoctoral Science Foundation (Grant No. 2022M712507), the Fundamental Research Funds for the Central Universities (Grant No. xzy01202003), and the National 111 Project of China (Grant No. B14040). The authors acknowledge the support from the Instrument Analysis Center of Xi'an Jiaotong University.

References

[1] Li J, Yi X, Hu W, *et al*. 2019 *Mater* **12** 2631
[2] Ha Y, Ts B, Wa Q, *et al*. 2020 *App. Sur. Sci.* **520** 146320
[3] Lu Q, Yu B, Hu Z Q, *et al*. 2020 *App. Sur. Sci.* **501** 144236
[4] Rodda S 1955 *Nature* **175** 1112
[5] Barut A O 1954 *Phys. Rev.* **93** 981
[6] Feng J F, Chen J Y, Venkatesan M, *et al*. 2010 *Phys. Rev. B* **81** 2498
[7] Chen Z, Chen X, Cui W Z, *et al*. 2015 *Journal of Infrared, Millimeter, and Terahertz Waves* **36** 430
[8] Khanm S S, Mao S, Zou Y, *et al*. 2023 *Vaccum* **215** 112257
[9] Spallino L, Angelucci M, Larciprete R 2019 *Appl. Phys. Lett.* **114** 153103
[10] Yang Z L, Yang J, He J, *et al*. 2023 *Chin. Phys. B* **32** 047901
[11] Wang F P, Zhao Q, Li J, Wang K Z, Huang Z Y and Cui W Z 2018 *Coatings* **8** 249
[12] Bai C and Cui W Z 2019 *International Journal of RF and Microwave Computer-Aided Engineering* **29** 21716
[13] Chen Z, Chen X, Cui W Z, *et al*. 2015 *Journal of Infrared, Millimeter, and Terahertz Waves* **36** 430
[14] Feng G, Liu L, Cui W Z, *et al*. 2020 *Chin. Phys. B* **29** 048703
[15] Noé J W 1993 *Nucl. Instrum. Methods Phys. Res. A* **328** 291
[16] Qi X, Ma Y Z, Liu S S, *et al*. 2023 *Coatings* **13** 1805
[17] Feng G B, Song H L, Li Y, *et al*. 2023 *Coatings* **13** 371
[18] Zhang H F, Ge Y, Lu M J, Zhang J C, *et al*. 2023 *Appl. Sur. Sci.* **15** 155789
[19] Feng G B, Liu L, Cui W Z, *et al*. 2020 *Chin. Phys. B* **29** 048703
[20] Pierron J, Inguimbert C, Belhaj M, Gineste T, Puech J and Raine M 2017 *J. Appl. Phys.* **64** 2340
[21] Pivi M, King F K, Kirby R E, *et al*. 2008 *J. Appl. Phys.* **104** 104904
[22] Wang Y, Zhang W, Wang S, *et al*. 2021 *J. Vac. Sci. Tech. B Nanotechnology and Microelectronics: Materials, Processing, Measurement, and Phenomena* **39** 34201
[23] Himpsel F J, Knapp J A, Vanvechten J A and Eastman D E 1979 *Phys. Rev. B* **20** 624
[24] Suetsugu Y, Tsuchiya M, Nishidono T, Kato N, Satoh N, Endo S and Yokoyama T 2003 *J. Vac. Sci. Tech. A Vac. Sur. Film.* **21** 186
[25] Liebendorfer A 2018 *Scilight* **2018** 220003
[26] Sattler J M, Jr R A C, Lake R, *et al*. 2017 *J. Appl. Phys.* **122** 055304
[27] Suetsugu Y, Tsuchiya M, Nishidono T, *et al*. 2003 *J. Vac. Sci. Tech. A Vac. Sur. Film.* **21** 186
[28] Ohyak, Itotani T and Kawata J 1994 *Jpn. J. Appl. Phys.* **33** 1153
[29] Luo J, Tian P, Pan C T, *et al*. 2011 *ACS Nano* **5** 1047
[30] Zhou M, *et al*. 2013 *Advanced Functional Materials* **23** 2263
[31] Bruining H 1962 *Physics & Applications of Secondary Electron Emission* **38** 78
[32] Lee M L, Fitzgerald E A, Bulsara M T, *et al*. 2005 *J. Appl. Phys.* **97** 011101
[33] Yang R, Qin Y, Dai L and Wang Z L 2009 *Nat. Nanotechnol.* **4** 34
[34] Ma J, Wer L, Bai Y, *et al*. 2021 *Thin Solid Films* **725** 138633
[35] Montero I, Aguilera L, Dávila M E, Nistor V C, González L A, Galán L, Raboso D and Ferritto R 2014 *Appl. Surf. Sci.* **291** 74
[36] Said K, Damamme G, Ahmed A S, *et al*. 2014 *Appl. Sur. Sci.* **297** 45
[37] Yang J, Cui W Z, Li Y, *et al*. 2016 *Appl. Sur. Sci.* **382** 88
[38] Zhang J Q, Chen J L, Ye M, Rao Z G, Shu L L, Hu Y M, Zeng X R and Ke S M 2019 *Appl. Surf. Sci.* **504** 144544
[39] Segall M D, Lindan P J D, Probert M J, *et al*. 2002 *J. Phys. Cond.* **14** 2717
[40] Dionne, Gerald F 1973 *J. Appl. Phys.* **44** 5361
[41] Dionne G F 1975 *J. Appl. Phys.* **46** 3347
[42] Young J R 1956 *J. Appl. Phys.* **27** 1
[43] Ye M, He Y N, Hu S G, *et al*. 2013 *J. Appl. Phys.* **113** 124404
[44] Shih A, Yater J, Pehrsson P, *et al*. 1997 *J. Appl. Phys.* **82** 1860
[45] Feng G B 2022 *Chin. Phys. B* **31** 107901
[46] Kitamura S, Suzuki K, Iwatsuki M, *et al*. 2000 *Appl. Sur. Sci.* **157** 222
[47] Li Y, Cui W Z, *et al*. 2017 *Chinese Space Science and Technology* **37** 73
[48] Chatterjee A 2006 *Molecular Simulation* **32** 155